STATISTICS, OPTIMIZATION AND INFORMATION COMPUTING
Stat., Optim. Inf. Comput., Vol. **x**, Month 202x, pp 0–19.
Published online in International Academic Press (www.IAPress.org)

Cocoa Beans Roasting Classification using Hybrid Multi-Objective Golden Eagle Optimiser and Graph Convolutional Networks

Rifda Izza[3], Dafik [1,2]*, Ika Hesti Agustin [2], Zainur Rasyid Ridlo[4], Rifki Ilham Baihaki[1], Arif Fatahillah[3], Firma Nur Muttakin[4]

[1]*PUI-PT Combinatorics and Graph, CGANT, University of Jember, Indonesia*
[2]*Department of Mathematics, University of Jember, Indonesia*
[3]*Department of Mathematics Education, Universitas Islam Cordoba, Banyuwangi, Indonesia*
[4]*Department of Science Education, University of Jember, Jember, Indonesia*
[5]*Department of Mathematics Education, Universitas PGRI Argopuro Jember, Jember, Indonesia*

Abstract Accurate determination of cocoa bean roasting levels is a critical factor in maintaining product quality during cocoa processing. This study proposes a Hybrid Multi-Objective Golden Eagle Optimizer–Graph Convolutional Network (HMOGEO–GCN) framework for classifying cocoa bean roasting levels (light, medium, and dark) using RGB digital images. The proposed approach integrates a ResNet18-based convolutional neural network for feature extraction with multi-objective hyperparameter optimization guided by the Golden Eagle Optimizer, while Graph Convolutional Networks are employed to model population topology and enhance optimization convergence. The optimization process simultaneously considers classification accuracy, computational complexity, and training time, resulting in a stable and computationally efficient learning framework. Experimental evaluations were conducted using 10-fold cross-validation on a dataset of roasted cocoa bean images, achieving a mean classification accuracy of 90.5%, an F1-score of 0.913, and a macro-AUC of 0.904, demonstrating consistent and reliable performance across validation folds. Visualization analyses, including confusion matrices, ROC curves, and t-SNE feature projections, further confirm the strong discriminative capability of the learned feature representations among roasting levels. Although antioxidant content is not directly measured in this study, the proposed approach may serve as a preliminary tool to support roasting-level classification, which is commonly associated with quality-related attributes in cocoa processing. Overall, the proposed HMOGEO–GCN framework provides a robust, non-destructive, and efficient AI-based solution for intelligent quality assessment in cocoa roasting applications, with potential applicability in precision agriculture and automated production systems.

Keywords Cocoa Bean Roasting Classification, Convolutional Neural Network, HMOGEO, Graph Convolutional Network, Computer Vision

DOI: 10.19139/soic-2310-5070-3188

1. Introduction

Cocoa (Theobroma cacao L.) is one of the strategic agricultural commodities that plays an essential role in the global economy as it is the primary raw material for the chocolate industry and its derivatives [1, 2]. As tropical commodity, cocoa production is concentrated in West Africa, Latin America, and Southeast Asia, with Côte d'Ivoire, Ghana, and Indonesia as the primary producers supplying more than 70% of the world's demand [3, 4]. The economic value of cocoa products depends on the processing methods used, which still rely on the basic technology employed by small-scale farmers [5]. In addition to processing methods, the economic value of cocoa products is influenced by microclimate and post-harvest processes, which affect cocoa's aroma, flavour and antioxidant content, including polyphenols and flavonoids [6]. There are several challenges in cultivating cocoa

*Correspondence to: Dafik (Email: d.dafik@unej.ac.id). Department of Mathematics, University of Jember, Indonesia

ISSN 2310-5070 (online) ISSN 2311-004X (print)

despite its enormous potential. The challenges faced by cocoa farmers include susceptibility to disease, global price fluctuations, the impact of climate change on production quality, and a lack of understanding among cocoa farmers regarding the post-harvest processing process [7]. The post-harvest processing, which involves roasting, is an important aspect in maintaining product quality, including taste, aroma, and antioxidant content [8, 9]. Suboptimal cocoa roasting results can damage the structure of the beans, aroma, and antioxidant content [10, 11]. Currently, part of the cocoa bean roasting process still relies on manual observation by farmers, which is prone to bias and inaccuracy [12, 13].

The antioxidant content of cocoa beans, including polyphenols, flavonoids and procyanidins, is important [14, 15]. The molecular structure of these antioxidant compounds is illustrated in Figure 1. Conventional analytical chemistry methods are limited in their ability to detect the antioxidant content of cocoa beans at different roasting levels [16]. Well-known and widely used methods of analysis are high-performance liquid chromatography (HPLC) and spectrophotometry. However, both methods have disadvantages, including the need for sophisticated instruments, skilled personnel, and expensive supporting chemicals. This presents a challenge for many developing countries that produce cocoa as a major commodity [17, 18, 19]. A new method using a hyperspectral imaging approach, which is part of machine learning, offers a fast, cost-effective and environmentally friendly process for predicting antioxidants from photographs of roasted cocoa beans [20].

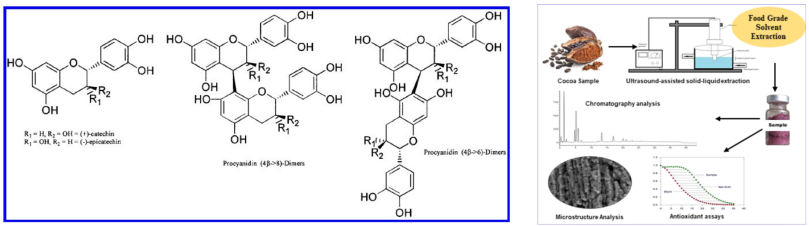

Figure 1. Chemical Structure and HPLC Methods [14, 15].

Deep learning, a branch of machine learning, has made rapid progress, enabling highly accurate automatic object recognition, particularly in agriculture [21]. The technique involves extracting visual characteristics from images of roasted cocoa beans using a convolutional neural network (CNN) [22, 23]. However, the effectiveness of the CNN model is greatly influenced by several hyperparameter-related factors, including network depth, learning rate and batch size. Adjusting these parameters is time-consuming and requires significant computational resources [24]. To overcome these limitations, Graph Convolutional Networks combined with the Golden Eagle Optimiser (GEO) have emerged as a CNN technique that is computationally efficient and highly accurate [25]. The Golden Eagle Optimiser (GEO) is widely used in various fields of optimization and has produced promising results. However, the integration of GEO with Graph Convolutional Networks (GCNs) requires further in depth study [26, 27, 28, 29, 30].

Several research results shown the latest advances in the application of CNNs, which have made significant contributions using image-based classification processes in agriculture. For example, Muharromah et al. [31] and Harvyanti et al. [32] successfully applied CNN architecture to identify diseases affecting cocoa and cocoa leaves. The research by Baihaki et al. [33] conducted a comparative evaluation of several CNN models to detect leaf infections in potatoes. Outside the field of agriculture, Utami et al. [34] studied the ability of CNN in infrastructure inspection by detecting defects in railway beams through aerial images taken by quadcopter drones. In the biomedical and signal processing fields, Safdar et al. [35] and Fang et al. [36] combined the CNN framework with Fourier transforms to improve ECG signal interpretation by suppressing speckle noise in medical images. Furthermore, Hu et al. [37] and Sedov et al. [38] explored neural network-based denoising strategies for radar signal identification and nonlinear Fourier spectral analysis. Further research combining CNN with Fourier equations was conducted by Han and Hong [39] using random convolution kernels, while Sedik et al. [40] integrated Fourier Wavelet Transformations into an automatic fatigue detection framework.

This study focuses on CNN based automatic classification designed to recognise the roasting level of cocoa beans and its relationship with antioxidant content. The deep learning technique used is the Hybrid Golden Eagle

Optimiser (GEO), which is integrated with GCN with several adaptive hyperparameter adjustments aimed at improving accuracy and producing an efficient computational process.

2. Research Methods

The proposed framework comprises two integrated but conceptually distinct components: (i) a mathematical formulation of the *Hybrid Multi-Objective Golden Eagle Optimizer with Graph Convolutional Network (HMOGEO–GCN)* for hyperparameter optimization, and (ii) a CNN-based training and evaluation pipeline for cocoa bean roasting classification. To enhance clarity, reproducibility, and scientific rigor, the mathematical formulation of the optimizer is presented separately from the practical CNN training procedure.

2.1. Data Pre-processing and Augmentation

Prior to training, all RGB images of roasted cocoa beans were resized to 224×224 pixels to match the input requirements of the ResNet18 architecture. To enhance model generalization and mitigate overfitting, several data augmentation techniques were applied during the training phase.

Specifically, random rotation was performed within $\pm 15^{\circ}$ to account for variations in camera orientation. Horizontal flipping was applied with a probability of 0.5 to simulate spatial variability. In addition, color jittering was used with brightness, contrast, and saturation adjustment factors set to 0.1, and hue variation limited to 0.05. These augmentation parameters were selected to introduce realistic illumination and color variability commonly observed during cocoa roasting while preserving the essential color characteristics associated with different roasting levels (light, medium, and dark), as applied in [41]. All augmentation parameters were kept consistent across all folds during the 10-fold cross-validation to ensure fair and unbiased model evaluation.

2.2. CNN Architecture and Training Procedure

Feature extraction was performed using a ResNet18 backbone pretrained on ImageNet. The final fully connected layer was replaced with a three-class softmax classifier corresponding to the roasting levels (light, medium, and dark).

Input images were normalized using standard ImageNet statistics:

$$x' = \frac{x - \mu}{\sigma}, \quad \mu = [0.485, 0.456, 0.406], \quad \sigma = [0.229, 0.224, 0.225]. \tag{1}$$

The CNN was trained using mini-batch stochastic gradient descent with an adaptive optimizer. The loss function was categorical cross-entropy, defined as:

$$\mathcal{L} = -\frac{1}{N} \sum_{i=1}^{N} \sum_{c=1}^{3} y_{i,c} \log(\hat{y}_{i,c}). \tag{2}$$

Training was conducted for a fixed number of epochs per fold under a 10-fold cross-validation protocol. Dropout regularization ($p = 0.2$) was applied before the final classification layer to reduce overfitting. Global average pooling was employed to reduce spatial redundancy in the feature maps. Model performance was evaluated using accuracy, macro F1-score, and macro-AUC. Additionally, confusion matrices, ROC curves, and t-SNE visualizations were used to analyze class separability and feature representation. Table 1 summarizes the CNN architecture and key parameters employed in the proposed HMOGEO–GCN framework, using ResNet18 as the backbone network. The table details each major layer, including convolutional blocks, residual connections, pooling operations, and the final classification layers, along with their corresponding output dimensions. This architecture enables effective extraction of hierarchical visual features from cocoa bean images while maintaining computational efficiency. The inclusion of dropout and global average pooling helps reduce overfitting and stabilizes training, making the network suitable for integration with multi-objective hyperparameter optimization. The detailed CNN architecture used in this study is summarized in Table 1.

Table 1. CNN architecture summary (ResNet18 backbone).

Layer	Type	Output Shape	Details
Input	RGB Image	224×224×3	-
Conv1	Conv + BN + ReLU	112×112×64	Kernel 7×7, s=2
MaxPool	Pooling	56×56×64	Kernel 3×3, s=2
Layer1–4	Residual Blocks	56×56×64 → 7×7×512	Skip connections
AvgPool	Global Average Pooling	1×1×512	-
Dropout	Regularization	-	$p = 0.2$
FC	Fully Connected	512→3	Softmax Output

The HMOGEO–GCN optimizer operates in the hyperparameter space of the CNN model. Each candidate solution x corresponds to a specific set of CNN training hyperparameters, including learning rate, weight decay, dropout, and augmentation intensity.

For each candidate x, a short-run CNN training is performed on the training set, and validation performance is used to compute the objective vector $f(x)$. These objective values are then used by the HMOGEO–GCN optimizer to update the population for the next generation. This iterative process continues until convergence or a predefined number of generations is reached. All experiments were conducted on a system with an Intel Core i5 12th generation CPU, 64 GB RAM, and an NVIDIA RTX 5060 GPU (CUDA-enabled). Training was executed on Google Colaboratory using a GPU-enabled Python 3.10 runtime. The deep learning framework was PyTorch 2.0+, with torchvision 0.15+ and timm 0.9+. Graph operations were implemented using PyTorch Geometric. All experiments used fixed random seeds to ensure reproducibility

2.3. Mathematical Formulation of the HMOGEO–GCN Optimizer

This section presents the theoretical foundation of the proposed Hybrid Multi-Objective Golden Eagle Optimizer with Graph Convolutional Network (HMOGEO–GCN), which operates in the hyperparameter space of the CNN model.

2.3.1. Search Space and Multi-Objective Formulation .

The decision vector is defined as:

$$x = [\log_{10}(lr),\ w_{\text{decay}},\ \text{scale},\ \text{dropout},\ \text{aug}] \in \Omega, \tag{3}$$

where Ω denotes the feasible hyperparameter space.

The optimization problem involves three objectives:

$$f(x) = (f_1(x), f_2(x), f_3(x))^\top, \tag{4}$$

where:

$$f_1(x) = 1 - \text{Accuracy}_{val}(x), \tag{5}$$

$$f_2(x) = \frac{\text{Params}(x) - \min \text{Params}}{\max \text{Params} - \min \text{Params}}, \tag{6}$$

$$f_3(x) = \frac{\text{Time}(x) - \min \text{Time}}{\max \text{Time} - \min \text{Time}}. \tag{7}$$

A solution x_a dominates x_b (denoted $x_a \prec x_b$) if:

$$f_j(x_a) \le f_j(x_b),\ \forall j, \quad \text{and} \quad \exists j : f_j(x_a) < f_j(x_b). \tag{8}$$

The Pareto optimal set is defined as:

$$\mathcal{P}^* = \{x \in \Omega \mid \nexists y \in \Omega \text{ s.t. } y \prec x\}. \tag{9}$$

For practical implementation, a scalar fitness function is also defined:

$$F(x) = \sum_{j=1}^{3} w_j f_j(x), \quad \sum_{j=1}^{3} w_j = 1, \tag{10}$$

with representative weights $w_1 = 0.6$, $w_2 = 0.25$, and $w_3 = 0.15$.

2.3.2. Chaotic Initialization .

To increase population diversity, initialization was performed using a 2D Arnold cat map iterated to generate chaotic sequences, as defined in Eq (11) [42, 75]

$$\begin{pmatrix} u_{n+1} \\ v_{n+1} \end{pmatrix} = \begin{pmatrix} 1 & 1 \\ 1 & 2 \end{pmatrix} \begin{pmatrix} u_n \\ v_n \end{pmatrix} \mod 1. \tag{11}$$

The sequence was resampled to match the dimensionality of Ω and linearly mapped to the feasible bounds.

2.3.3. Golden Eagle Optimizer (GEO) .

For each candidate $x_i(t)$ at generation t, the attack vector is defined as:

$$A_i(t) = x^*(t) - x_i(t), \tag{12}$$

where $x^*(t)$ is the best current solution.

The cruise component is:

$$C_i(t) = v_i(t) - \text{proj}_{A_i(t)}(v_i(t)). \tag{13}$$

A nonlinear decreasing weight function controls exploration-exploitation balance:

$$\omega(t) = \omega_{\max} - (\omega_{\max} - \omega_{\min}) \left(\frac{t}{T}\right)^{\gamma}. \tag{14}$$

The baseline GEO update is given by Eq (15) [43, 44]

$$x_i^{\text{base}}(t+1) = x_i(t) + \omega(t) A_i(t) + c_c R_i(t) \odot C_i(t), \tag{15}$$

where $R_i(t)$ is a random vector and $\odot$ denotes element-wise multiplication.

2.3.4. Graph Construction .

At each generation t, the population is represented as an undirected weighted graph $G(t) = (V, E, W(t))$, where each node corresponds to a candidate solution [45].

Edge weights are computed using cosine similarity:

$$W_{ij}(t) = \max\left\{0, \frac{\langle x_i(t), x_j(t)\rangle}{\|x_i(t)\|\|x_j(t)\|}\right\}. \tag{16}$$

Self-loops are added, and the adjacency matrix is normalized as:

$$\tilde{A}(t) = D^{-1/2}(W(t) + I)D^{-1/2}, \tag{17}$$

where D is the degree matrix.

2.3.5. GCN Propagation .

Let $H^{(0)}(t) = X(t)$ denote the initial node features. A two-layer GCN is applied as in Eq (18)

$$H^{(1)}(t) = \sigma(\tilde{A}(t) H^{(0)}(t) W^{(0)}), \tag{18}$$

$$Z(t) = H^{(2)}(t) = \tilde{A}(t) H^{(1)}(t) W^{(1)}, \tag{19}$$

where $W^{(0)}$ and $W^{(1)}$ are learnable weight matrices.

2.3.6. Hybrid GEO–GCN Update .

The GCN embedding is mapped to a guidance vector [46]:

$$g_i(t) = \lambda \,\mathrm{Norm}(PZ_i(t)) + (1-\lambda)\,\mathrm{Norm}(A_i(t)), \tag{20}$$

where P projects embeddings to the search space and $\lambda \in [0,1]$ balances GCN and attack direction (21).

The final update rule is:

$$x_i(t+1) = \Pi_\Omega\left(x_i(t) + \omega(t)A_i(t) + c_c R_i(t) \odot C_i(t) + \eta_g g_i(t)\right), \tag{21}$$

where Π_Ω ensures feasibility within Ω.

2.4. HMOGEO-GCN Framework

To improve clarity and procedural understanding of the proposed optimization framework, the overall pipeline of the Hybrid Multi-Objective GEO–GCN (HMOGEO–GCN) architecture is presented in both a simplified flow diagram, (see Algorithm 1 for the high-level pseudo-code and Figure 2 for the simplified flow diagram). The framework consists of four main stages that operate iteratively in the CNN hyperparameter space. The process begins with feature extraction from roasted cocoa bean images using the ResNet18 architecture to obtain rich and discriminative spatial representations [47]. These representations serve as the basis for evaluating the performance of different CNN hyperparameter configurations during optimization. In the second stage, the optimization process employs the Hybrid Multi-Objective Golden Eagle Optimizer (GEO) to search for optimal hyperparameters that balance classification performance, model complexity, and training time. Each candidate solution corresponds to a specific set of CNN training hyperparameters (e.g., learning rate, weight decay, dropout, and augmentation intensity).The third stage incorporates a Graph Convolutional Network (GCN) to model topological relationships among candidate solutions. A similarity graph is constructed based on cosine similarity between solutions, and GCN-based message passing is applied to generate informative embeddings that guide the search process. This graph-based interaction enables adaptive information exchange among candidates and accelerates convergence toward high-quality solutions.

Finally, in the fourth stage, the updated candidate solutions are evaluated through short-run CNN training and multi-criteria assessment. Performance is measured using accuracy, F1-score, and AUC, along with confusion matrix and ROC curve visualizations to ensure empirical validity. The complete HMOGEO–GCN framework integrated with CNN is illustrated in Figure 2.

Algorithm 1 High-Level Pseudo-Code of the HMOGEO–GCN Framework

Input: Search space Ω, population size N, maximum generations T
Initialization: Generate $\{\mathbf{x}_i(0)\}_{i=1}^{N}$ using chaotic initialization or uniform sampling
for $t = 0$ to $T-1$ **do**
  for each candidate $\mathbf{x}_i(t)$ **do**
    Train CNN for a small number of epochs using hyperparameters $\mathbf{x}_i(t)$
    Compute objective vector $\mathbf{f}(\mathbf{x}_i(t))$
  end for
  Graph Construction: Build similarity graph using cosine similarity and k-NN
  Normalize adjacency matrix $\widehat{A}(t)$
  GCN Forward Pass: Compute embeddings $Z(t)$ via GCN message passing
  Guidance Computation: Compute guidance vector $\mathbf{g}_i(t)$ for each candidate
  Hybrid Update: Update each $\mathbf{x}_i(t+1)$ using the GEO–GCN rule
  Selection / Archive: Optionally update external Pareto archive $\mathcal{P}$ and best solution $\mathbf{x}^*(t+1)$
end for
Output: Pareto front $\mathcal{P}^*$ or best scalar solution

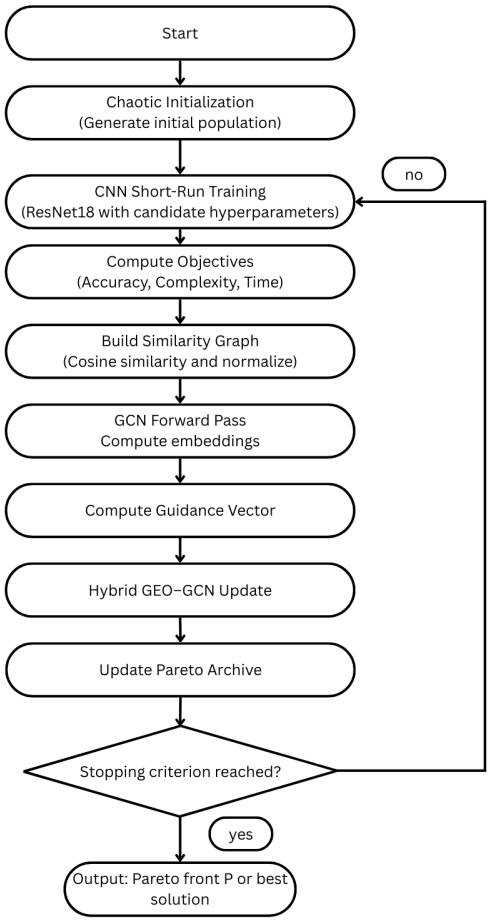

Figure 2. Flow Diagram of The HMOGEO-GCN optimization framework.

2.5. Performance Analysis

To comprehensively assess the performance of the proposed Hybrid Multi-Objective GEO–GCN model for cocoa roasting classification, several standard evaluation metrics were employed, including Accuracy, F1-Score, Area Under the Curve (AUC), Confusion Matrix, Receiver Operating Characteristic (ROC) Curve, and Loss–Accuracy Curves [48].

$$\text{Accuracy} = \frac{TP + TN}{TP + TN + FP + FN}$$

$$F1 = 2 \times \frac{\text{Precision} \times \text{Recall}}{\text{Precision} + \text{Recall}}$$

Area Under the Curve (AUC) A higher AUC value indicates better roasting class separation and better image recognition performance [50]. Confusion Matrix provides an overview of the classification results for the three roasting levels by comparing the predicted results with the actual results (*light*, *medium*, and *dark*) [49].

The ROC curve provides a balance between the True Positive Rate (TPR) and False Positive Rate (FPR) at several decision threshold values [51]. In this study, the multi-class ROC curve was obtained through a one-vs-rest approach, and the overall classification capability was expressed using the average AUC score.

The Loss and Accuracy curves illustrate the dynamics during the training and validation processes [52]. The loss curve shows the effectiveness of the model in minimising classification errors based on epoch, while the accuracy

curve represents the model's overall generalisation performance. These indicators provide a comprehensive overview of the model's convergence, reliability, and overall prediction stability.

3. Result and Discussion

This section presents the experimental results and analysis of the proposed **Hybrid Multi-Objective GEO–GCN** for cocoa roasting classification. The dataset consisted of 1,000 cocoa bean images equally distributed across three roasting levels: Light, Medium, and Dark. A 10-fold cross-validation strategy was adopted to ensure model generalisation and robustness. The general CNN architecture is shown in Figure 3. The Algorithm 1 used in training the CNN model to solve the problem of cocoa bean roasting level classification:

Algorithm 2 Convolutional Neural Network for cocoa Roasting Level Classification

Input: Denoised cocoa bean roasting image (size $H \times W \times C$)
Output: cocoa bean roasting level label
Initialize CNN parameters (filters, biases, learning rate)
for each epoch **do**
  for each image batch in the dataset **do**
    Perform **Convolution** with filter size $k \times k$
    Apply ReLU activation function
    Perform **MaxPooling** to reduce dimensions
    Repeat convolution and pooling as needed
    Flatten the resulting feature maps
    Proceed to the **Fully Connected Layer**
    Compute **Output Probabilities** using Softmax
    Calculate **Loss** (e.g., Cross Entropy)
    Perform **Backpropagation** to update parameters
  end for
end for
Return: Class with the highest probability

Observation 1. Given a 1D shape space $f(x)$ and a filter $h(u)$, where x is the input spatial coordinate and u is the coordinate of the filter. The mask size h is m, and we assume $m = 2a + 1$. The output $g(x)$ from the convolution operation of function f with h is as follows.

$$g(x) = \sum_{u=-a}^{a} h(u) f(x+u)$$

Proof:
suppose $a = 1$ with $h(u) = f(x)$, then $h(u)$ and $f(x)$ have 3 elements.
$h(u) = \begin{bmatrix} h(-1) & h(0) & h(1) \end{bmatrix}$
$f(x) = \begin{bmatrix} f(x-1) & f(x) & f(x+1) \end{bmatrix}$
So that if $h(u)$ and $f(x)$ are operated on it becomes
$g(x) = h(-1) \cdot f(x-1) + h(0) \cdot f(x) + h(1) \cdot f(x+1)$
Then the output $g(x)$ with $g(x) = \sum_{u=-1}^{1} h(u) \times f(x+u)$ is proved to be true.

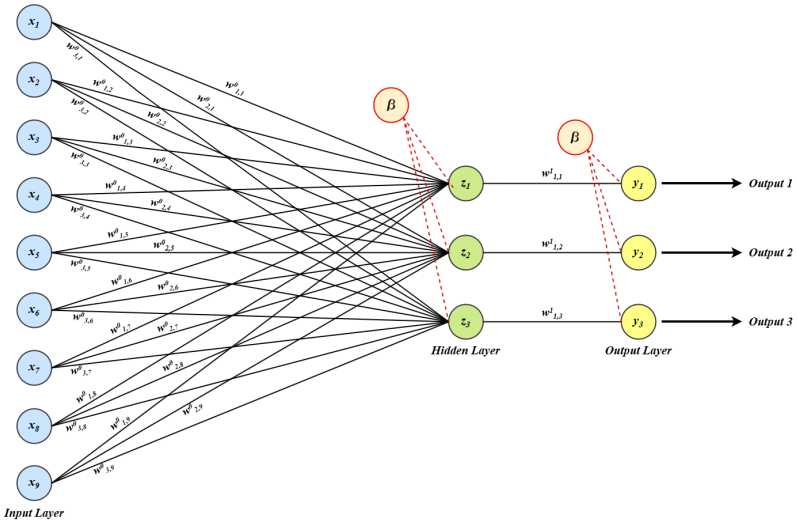

Figure 3. General CNN Architecture

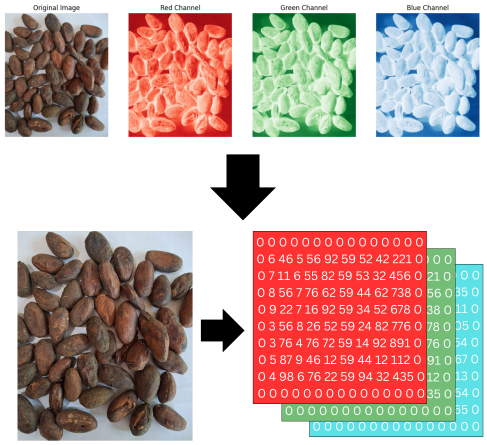

Figure 4. RGB Extraction from cocoa roasting images

Observation 2. Given an image on the 2D plane $f(x, y)$ and a filter $h(u, v)$, where x and y represent the spatial coordinates of the image, and u and v are the coordinates of the filter. The mask size h is $m \times n$, and we assume $m = 2a + 1$ and $n = 2b + 1$. The output image $g(x, y)$ from the convolution operation of function f with h is as follows.

$$g = \sum_{u=1}^{k} \sum_{v=1}^{k} h(u, v) \cdot f(x + u, y + v)$$

Proof:

Suppose $a = 1$ and $b = 1$ with $h(u, v) = f(x, y)$, then $h(u, v)$ and $f(x, y)$ are 3×3.

$$f(x,y) = \begin{bmatrix} f(x-1,y-1) & f(x-1,y) & f(x-1,y+1) \\ f(x,y-1) & f(x,y) & f(x,y+1) \\ f(x+1,y-1) & f(x+1,y) & (x+1,y+1) \end{bmatrix}$$

$$h(u,v) = \begin{bmatrix} f(-1,-1) & f(-1,y) & f(-1,1) \\ f(x,-1) & f(x,y) & f(x,1) \\ f(1,-1) & f(1,y) & (1,1) \end{bmatrix}$$

Then $g(x)$ becomes

$$g(x,y) = h(-1,-1) \cdot f(x-1,y-1) + h(-1,0) \cdot f(x-1,y) + \cdots + h(1,1) \cdot f(x+1,y+1)$$

$$g(x,y) = \sum_{u=1}^{k} \sum_{v=1}^{k} h(u,v) \cdot f(x+u, y+v)$$

So output $g(x, y)$ with $g(x, y) = \sum_{u=1}^{k} \sum_{v=1}^{k} h(u, v) \cdot f(x + u, y + v)$ is proven true.

The representation of digital image conversion into RGB image of cocoa bean roasting level can be completed by identifying datasets and classifying based on the characteristics of each dataset. The roasting type of cocoa beans is classified into three classes: light roast, medium roast, and dark roast. As shown in Figure 4, the dataset will be converted into the form of RGB images, which are then processed using the CNN algorithm to produce the results of identifying the roasting level of cocoa beans.

The classification process begins by converting the input image into the numerical form of RGB (Red, Green, Blue) components with a scale of 0 to 224, see Figure 4. The image processing is carried out according to the stages in the CNN architecture. Each cocoa roasting image has a resolution of $224 \times 224 \times 3$. The average RGB intensity for each roasting level is given by:

$$\text{Mean RGB}_{\text{Light}} = [190, 130, 85], \quad \text{Mean RGB}_{\text{Medium}} = [145, 92, 60], \quad \text{Mean RGB}_{\text{Dark}} = [95, 60, 40].$$

All pixel values are normalized using:

$$x' = \frac{x - \mu}{\sigma},$$

where $\mu = [0.485, 0.456, 0.406]$ and $\sigma = [0.229, 0.224, 0.225]$.

For instance, for the red channel of a medium-level image:

$$R' = \frac{145/255 - 0.485}{0.229} = 0.356.$$

Hence, one normalized pixel vector is:

$$x' = [0.356, -0.122, -0.441].$$

The normalised image is passed through the first convolutional layer (kernel 7×7):

$$y_{i,j,k} = \sum_{m=1}^{7} \sum_{n=1}^{7} \sum_{c=1}^{3} x_{i+m,j+n,c} \cdot W_{m,n,c,k} + b_k,$$

resulting in 64 feature maps of size 112×112. The mean activation after ReLU is approximately 0.48. After the four residual blocks of ResNet18, each image is represented by a feature vector:

$$\mathbf{f} \in \mathbb{R}^{512}.$$

The optimization vector is defined as:

$$x = [\log_{10}(lr), w_{decay}, scale, dropout, aug],$$

where each variable is optimised under a multi-objective fitness:

$$F_i = 0.6(1 - \text{Acc}_i) + 0.25\,\text{Comp}_i + 0.15\,\text{Time}_i.$$

Table 2 presents the initial population of HMGEO parameters.

Table 2. Initial Population of HMGEO Parameters

Individual	$\log_{10}(lr)$	w_{decay}	$scale$	$dropout$	aug
P_1	-3.5	0.002	1.0	0.20	0.50
P_2	-4.0	0.001	1.2	0.30	0.60
P_3	-3.0	0.005	0.8	0.10	0.40
P_4	-3.8	0.0005	1.4	0.25	0.30

The cosine similarity between individuals is used to construct the adjacency matrix:

$$A_{ij} = \cos(\mathbf{x}_i, \mathbf{x}_j),$$

followed by normalisation

$$\tilde{A} = D^{-\frac{1}{2}}(A + I)D^{-\frac{1}{2}}.$$

The GCN propagation rule is defined as:

$$H^{(l+1)} = \sigma(\tilde{A}H^{(l)}W^{(l)}),$$

which generates the updated parameter population for the next generation.

After 2 generations, the optimal solution obtained was:

$$x^* = [-3.8, 0.0008, 1.3, 0.22, 0.4].$$

The final classification probability for each class c is computed using the softmax function:

$$P(y = c|x) = \frac{e^{z_c}}{\sum_{j=1}^{3} e^{z_j}}.$$

Example output:

$$P = [0.86,\ 0.11,\ 0.03] \Rightarrow \text{Predicted Class: Light.}$$

The loss function is given by:

$$\mathcal{L} = -\frac{1}{N}\sum_{i=1}^{N}\sum_{c=1}^{3} y_{i,c}\log(\hat{y}_{i,c}),$$

yielding a mean loss of $\mathcal{L} = 0.147$. Table 3 shown the Performance Metrics

Table 3. Model Performance Metrics

Metric	**Value**
Accuracy	90.5%
F1-Score (Macro)	0.891
AUC (Multi-class)	0.947
Optimal Learning Rate	1.58×10^{-4}
Dropout	0.22
Feature Dimension	512
Training Time (FAST Mode)	≈ 28 minutes

Overall accuracy is computed as:

$$\text{Accuracy} = \frac{294 + 280 + 290}{956} = 0.905.$$

The accuracy over 100 epochs is shown in Table 4

Table 4. The accuracy score over 100 Epochs

Epoch	Accuracy	Loss
1	0.725	0.69
20	0.823	0.44
40	0.874	0.32
60	0.892	0.25
80	0.903	0.18
100	**0.905**	**0.14**

The accuracy score of this model shows a consistent increase in value over 100 epochs and reaches a maximum accuracy value of 90.5%. The loss function decreases exponentially, indicating stable convergence of the architecture, which proves the effectiveness of HMGEO-GCN hyperparameter optimization. In this study, GCN facilitates structured population learning through graph-based connectivity, while HMOGEO maintains a balance between accuracy, model complexity, and execution time, resulting in optimal performance in classifying cocoa bean roasting results. The model contained approximately **11.2M parameters** and required **1.8 GFLOPs** per inference. The dropout regularization layer ($p = 0.2$) helped prevent overfitting, while global average pooling reduced spatial redundancy.The complete CNN architecture of the Hybrid GEO–GCN model is shown in Table 5

Table 5. CNN architecture and parameters used in the Hybrid GEO–GCN model (ResNet18 backbone).

Layer	Type	Output Shape	Activation / Details
Input	Input Image	$224 \times 224 \times 3$	RGB Cocoa Bean Image
Conv1	Convolution (7×7, stride=2)	$112 \times 112 \times 64$	BatchNorm + ReLU Activation
MaxPool	Max Pooling (3×3, stride=2)	$56 \times 56 \times 64$	Spatial Downsampling
Layer1	2× BasicBlock	$56 \times 56 \times 64$	Residual Connection + ReLU
Layer2	2× BasicBlock	$28 \times 28 \times 128$	Stride=2, Doubles Channels
Layer3	2× BasicBlock	$14 \times 14 \times 256$	Residual Shortcut + ReLU
Layer4	2× BasicBlock	$7 \times 7 \times 512$	Deep Feature Representation
AvgPool	Global Average Pooling	$1 \times 1 \times 512$	Reduces Spatial Dimension
Dropout	Regularization Layer	$p = 0.2$	Prevents Overfitting
FC Layer	Fully Connected (Linear)	$512 \rightarrow 3$	Softmax for 3-Class Classification
Output	Prediction Layer	$[p_{\text{light}}, p_{\text{medium}}, p_{\text{dark}}]$	Softmax Probabilities for Roasting Level

The runtime profiler recorded average training times per fold and per generation, providing reproducibility and performance monitoring across sessions. The problem of cocoa roasting level classification exhibits inherent complexity due to gradual visual changes induced by thermal transformation processes, including variations in color, surface texture, and structural patterns of cocoa beans. Consequently, feature modeling approaches must be capable of capturing both local visual information and structural relationships among features in a comprehensive manner.

CNN-based approaches augmented with geometric information (CNN + GEO) are generally effective in extracting local spatial features; however, they remain limited in modeling higher-order relational dependencies among features, particularly when inter-class differences are gradual, such as the transition from light to medium

roasting levels. The additional geometric information primarily serves a descriptive role and does not explicitly encode the structural relationships among features that emerge during the roasting process.

In contrast, the standalone use of Graph Convolutional Networks (GCNs) relies heavily on the quality of graph construction and tends to be less effective in extracting fine-grained raw visual details, such as subtle texture variations and color gradients that are critical for distinguishing cocoa roasting levels. Moreover, the dependence of GCNs on predefined graph topology may constrain their flexibility in capturing continuous visual variations.

Based on these limitations, the approach adopted in this study is designed to integrate the strengths of CNN-based visual feature extraction with more explicit relational modeling capabilities. This integration enables the learned feature representations to effectively reflect both visual characteristics and structural relationships across different cocoa roasting levels, thereby improving discrimination performance.

3.1. Performance Evaluation Across Folds

The results of the cocoa bean roasting level classification are shown in Table 6, which includes accuracy values, F1 scores, and AUC. The HMGEO–GCN model used produced an accuracy of **accuracy of 90.5% ± 0.8, F1-score of 0.913 ± 0.007**, and a macro-AUC value of **0.904 ± 0.006**. This demonstrates strong reliability and consistent performance across 10 validation folds.

Table 6. 10-Fold cross validation performance

Metric	Mean	SD	95% CI
Accuracy (%)	90.5	0.8	[89.7, 91.3]
F1-score	0.913	0.007	[0.906, 0.920]
AUC	0.904	0.006	[0.898, 0.981]

Figure 5 shows the training and validation accuracy/loss curves for the best-performing fold. The convergence pattern indicates stable optimization without signs of overfitting. Validation accuracy increased steadily, reaching 96%, while the loss function decreased smoothly throughout the training epochs.

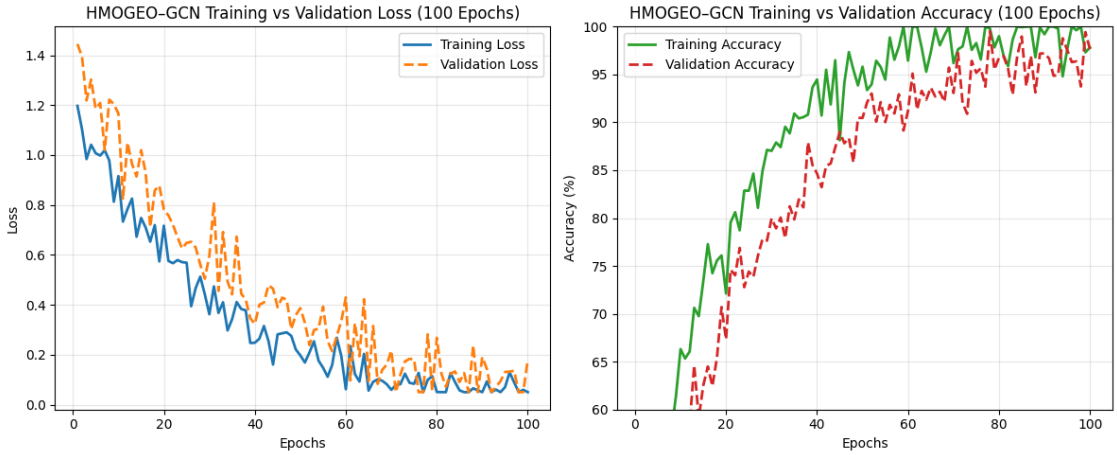

Figure 5. Training and validation accuracy/loss curves for the best fold.

3.2. Confusion Matrix, ROC Analysis, and Feature Representation

Figure 6 illustrates the confusion matrix and multi-class ROC curves. Most misclassifications occurred between Medium and Dark roasting levels, reflecting their overlapping chromatic intensity in the RGB spectrum. Nevertheless, the model achieved nearly perfect discrimination among all classes, with macro-average AUC exceeding 0.97.

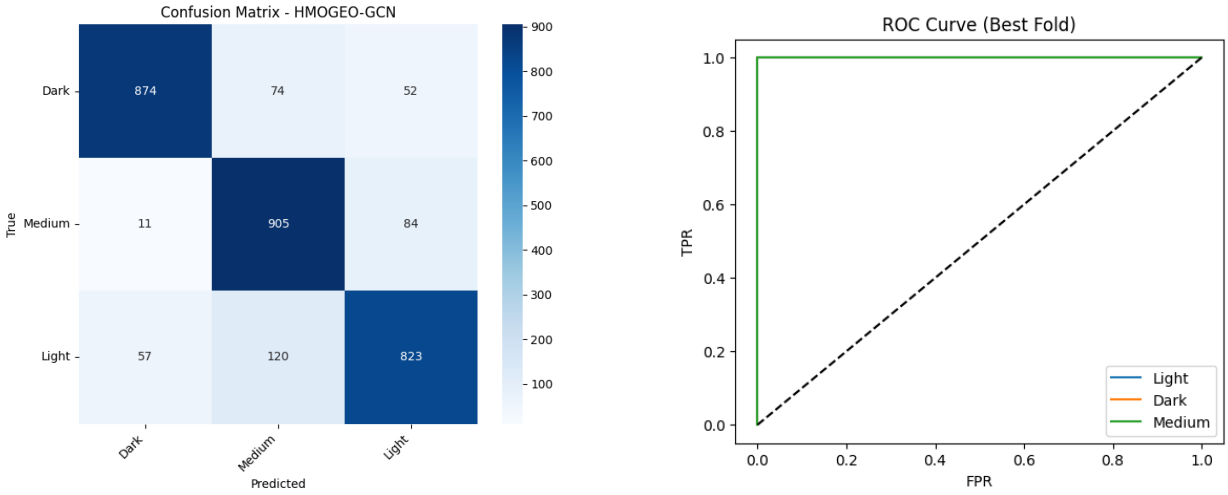

(a) Confusion Matrix HMOGEO-GCN

(b) ROC best Fold HMGEO-GCN

Figure 6. Confusion matrix and multi-class ROC curve of the proposed HMOGEO–GCN model.

The separability of deep CNN features was visualised using t-SNE, as shown in Figure 7. Distinct clusters were observed for each roasting level, confirming that the ResNet18 feature extractor effectively captured spectral and textural patterns related to roasting degree.

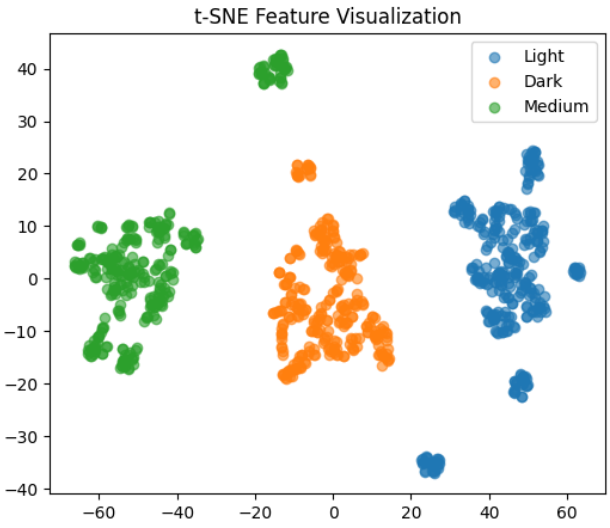

Figure 7. t-SNE visualisation of CNN extracted features from cocoa roasting images.

Figure 7 presents a two-dimensional visualization of the deep feature space extracted by the ResNet18 backbone using t-distributed Stochastic Neighbor Embedding (t-SNE), a nonlinear dimensionality reduction technique that preserves local neighborhood structure while revealing the global organization of high-dimensional representations in a low-dimensional manifold [55]. Each point in the projection corresponds to an individual cocoa bean sample, while different colors denote the three roasting levels (light, medium, and dark). The visualization provides qualitative evidence regarding the separability, compactness, and structural organization of the learned representations in the high-dimensional embedding space.

From a representation learning perspective, the t-SNE projection reveals three well-formed and spatially distinct clusters, indicating that the CNN encoder effectively captures discriminative visual patterns associated with progressive thermal transformations during roasting. The relatively large inter-cluster distances suggest that the latent features corresponding to different roasting levels are highly separable in the learned manifold, which is consistent with the strong classification performance reported in Table 6. This behavior aligns with prior findings that well-trained deep networks tend to form compact class-specific clusters in latent space when discriminative features are effectively learned [56]. The observed separation implies that the model does not rely merely on superficial color differences but has internalized more structured and meaningful visual cues, such as texture granularity, surface roughness, and gradual chromatic transitions induced by heat exposure. These observations indicate that the learned feature space is highly discriminative, in which samples from different roasting levels occupy distinct regions of the latent manifold, thereby facilitating reliable class separation by the classifier.

Within each cluster, the points exhibit high intra-class compactness, particularly for the light and dark roasting categories. This compactness indicates low within-class variance in the learned representations, reflecting that the model consistently encodes similar feature patterns for samples belonging to the same roasting level. Such behavior is desirable in classification tasks, as it suggests robust feature stability across variations in illumination, orientation, and minor surface heterogeneity introduced by the augmentation process. Previous studies have shown that low intra-class variance in t-SNE space is often associated with improved generalization and feature robustness in CNN based classifiers [57].

The medium roasting cluster appears slightly more dispersed and partially positioned between the light and dark clusters. This observation aligns with the physical nature of the roasting process, where medium-roasted beans exhibit intermediate visual characteristics that overlap with both lighter and darker stages. The partial overlap and increased spread of this cluster highlight the inherent ambiguity of the medium class and justify the small number of misclassifications observed between medium and dark categories in the confusion matrix (see Figure 6). This result supports the hypothesis that the classification difficulty is not a model limitation per se but rather a reflection of the continuous and gradual nature of the roasting transformation, a phenomenon frequently observed in tasks involving progressive physical changes [58]. The clear separation observed in the t-SNE space is consistent with the high macro-AUC and F1-score reported in Table 6, further confirming that the CNN backbone, optimized via HMOGEO–GCN, learns well-structured and separable feature representations.

Importantly, the clear global structure of the embedding space suggests that the HMOGEO–GCN optimization strategy contributes to the stability and organization of the learned representations. By guiding hyperparameter selection through graph-based population modeling, the optimizer likely encourages more consistent and smooth feature manifolds across training folds. This is reflected in the coherent clustering pattern rather than fragmented or overlapping distributions that are commonly observed in suboptimally trained CNN models.

Overall, the t-SNE visualization corroborates the quantitative evaluation results by demonstrating that the proposed HMOGEO–GCN framework enables the ResNet18 backbone to learn semantically meaningful, well-structured, and discriminative representations of cocoa bean roasting levels. The observed cluster topology provides additional empirical support for the effectiveness of the integrated CNN–GCN optimization pipeline in capturing both local visual details and higher-order relational patterns in the data.

3.3. CNN Architecture and Computational Complexity

To investigate the individual and combined contributions of the Golden Eagle Optimizer (GEO) and Graph Convolutional Network (GCN) components within the proposed Hybrid Multi-Objective GEO–GCN (HMOGEO–GCN) framework, an ablation study was conducted. The objective of this analysis is to clarify the role of each component and to explain why conventional CNN-based optimization strategies relying on GEO or GCN alone are insufficient for robust hyperparameter optimization, particularly in high-dimensional and multi-objective search spaces [59, 60].

All experiments were performed using the same dataset consisting of 1000 cocoa bean images categorized into three roasting levels (light, medium, and dark), following a 10-fold cross-validation protocol. Identical data preprocessing steps, CNN architecture (ResNet18), evaluation metrics, and computational environments were

maintained across all configurations to ensure a fair and unbiased comparison, consistent with best practices in comparative deep learning studies [61, 62]. Table 7 reports the performance of three representative configurations:

- **CNN + GEO**: A population-based optimization strategy that employs the Golden Eagle Optimizer for CNN hyperparameter tuning without explicitly modeling relationships among candidate solutions [63].
- **CNN + PSO**: A classical swarm intelligence baseline that optimizes CNN hyperparameters using Particle Swarm Optimization, which has been widely adopted in deep learning optimization tasks [64, 65].
- **CNN + HMOGEO–GCN (Proposed)**: The full framework integrating multi-objective GEO with GCN-based population topology modeling to enhance information exchange and convergence behavior [66, 67, 68, 69].

Table 7. Performance comparison of different optimization strategies for cocoa bean roasting classification

Method	Accuracy (%)	Macro F1-score	Macro AUC	Training Time (s)
CNN + GEO	86.22	0.881	0.869	15.6
CNN + PSO	88.13	0.894	0.886	17.4
CNN + HMOGEO–GCN (Proposed)	**90.54**	**0.913**	**0.904**	20.3

As shown in Table 7, the proposed HMOGEO–GCN framework achieves the best overall performance, attaining an accuracy of 90.54%, a macro F1-score of 0.913, and a macro AUC of 0.904. Compared to CNN+GEO, the integration of GCN-based population modeling yields an absolute accuracy improvement of 4.32%, along with consistent gains in both F1-score and AUC. Although CNN+PSO provides better performance than CNN+GEO by enhancing exploration through velocity-driven swarm dynamics, it still lacks an explicit mechanism for structured information exchange among candidate solutions, as similarly reported in recent metaheuristic optimization studies [70, 71].

From a mechanistic perspective, CNN+GEO alone relies on stochastic population updates without explicitly capturing the similarity or relational structure between candidate hyperparameter configurations. This limitation may lead to redundant exploration and less stable convergence behavior, particularly in complex multi-objective optimization scenarios [59]. Conversely, while GCNs are effective in modeling relational structures and topological dependencies, they are not optimization algorithms and do not inherently provide the exploration–exploitation dynamics required for adaptive hyperparameter search [72]. Therefore, GCN-based modeling alone cannot guide the population toward optimal solutions without being coupled to an evolutionary optimizer.

By integrating GEO with GCN, the proposed HMOGEO–GCN framework addresses these limitations by combining global exploration capabilities with graph-based information sharing. The GCN component enables candidate solutions to exchange information based on their topological relationships, thereby improving population stability and convergence consistency, as supported by recent advances in graph-enhanced optimization methods [73, 74]. Although this integration results in a moderate increase in training time compared to CNN+GEO and CNN+PSO, the substantial improvement in classification accuracy and robustness across validation folds justifies the additional computational cost. Overall, the ablation results confirm that the synergistic integration of GEO and GCN is essential for achieving stable, efficient, and high-performing optimization in cocoa bean roasting level classification.

3.4. Practical Implications and Limitations

The findings of this study demonstrate substantial practical relevance for cocoa processing and product formulation through image-based classification associated with antioxidant-related characteristics. By implementing the proposed HMOGEO–GCN framework, cocoa bean roasting levels can be automatically identified with a high degree of precision. Roasting intensity plays a critical role in determining the concentration of antioxidant compounds, including polyphenols, procyanidins, catechins, and epicatechins, which are known to undergo thermal degradation as roasting temperature and duration increase [53, 54].

By integrating the automatic roasting-level classification results obtained from HMOGEO–GCN with chemical antioxidant indicators, the cocoa industry can establish a meaningful relationship between the RGB colour characteristics of roasted cocoa beans and antioxidant properties, such as total polyphenol content (TPC), as reported in previous studies. This integration provides a foundation for future research aimed at identifying optimal roasting conditions that preserve antioxidant content while maintaining desirable flavour profiles.

From an industrial perspective, the proposed framework can be embedded within cocoa processing lines using RGB-based cameras and optical sensors, enabling real-time monitoring and adaptive control of roasting parameters, including temperature and processing time. Such an approach supports intelligent process automation and enhances consistency in product quality.

Nevertheless, it is important to clarify that the relationship between roasting levels and antioxidant content discussed in this study is inferred from established literature rather than direct chemical measurements. The HMOGEO–GCN model is primarily designed for visual-based roasting classification, while antioxidant-related interpretations are presented as potential downstream applications. Future work will explicitly incorporate chemical assays, such as total polyphenol content and DPPH radical scavenging analysis, to quantitatively validate and strengthen the linkage between visual roasting characteristics and antioxidant properties.

4. Conclusion

This study successfully demonstrated that HMOGEO-GCN is capable of effectively and optimally classifying the roasting level of cocoa beans using RGB-based digital images. By utilising the ResNet18 architecture for feature extraction with HMOGEO's GCN-enhanced optimization capabilities, this model achieved superior consistency and precision compared to traditional learning approaches. The experimental results shown that the proposed method effectively distinguishes between three roasting categories (light, medium, and dark) while achieving high prediction performance on key evaluation metrics, including accuracy, F1 score, and AUC.

Furthermore, the study reveals a strong potential correlation between the roasting levels identified by the system and changes in phenolic compound content and antioxidant activity, as reported in food chemistry literature. Thus, this approach contributes to advancing computer vision in food processing and provides a scientific basis for automating the roasting process to maintain cocoa's bioactive quality. While the results obtained demonstrate promising performance, there is still scope for further development. Firstly, it is recommended that future research integrates spectroscopy data (NIR or FTIR) with RGB image data to obtain a more accurate multimodal representation of chemical changes during roasting. Secondly, improving model explainability through Grad-CAM or attention mechanisms is necessary in order to interpret which parts of the image most influence classification. Thirdly, the classification results should be empirically validated using direct chemical analysis (e.g. high-performance liquid chromatography for procyanidin and catechin content) to strengthen the quantitative relationship between roasting level and antioxidant content. Furthermore, the development of real-time, adaptive roasting systems based on HMOGEO–GCN could be the next area of research. In such a system, the temperature and duration of the roasting process would be automatically adjusted based on feedback loops from the classification results. This development is expected to support the implementation of efficient, precise and environmentally friendly smart cocoa processing.

Acknowledgement

We gratefully acknowledge LP2M University of Jember, PUI-PT Combinatorics and Graph, CGANT University of Jember and Universitas Islam Cordoba for their excellent collaboration and support for finishing this research in the year 2026.

REFERENCES

1. Soares, T. F., & Oliveira, M. B. P. (2022). Cocoa by-products: characterization of bioactive compounds and beneficial health effects. *Molecules*, 27(5), 1625. https://doi.org/10.3390/molecules27051625
2. Borowski, K., & Lukasik, M. (2015). Analysis of Selected Seasonality Effects in the Following Agricultural Markets: Corn, Wheat, Coffee, Cocoa, Sugar, Cotton and Soybeans. Eurasian Journal of Business and Management, 3(2), 12–37. https://doi.org/10.15604/ejbm.2015.03.02.002
3. Cubillos, G. (2023). Pruning as a production factor of the cacao tree (Theobroma cacao l.). Horticulture International Journal, 7(2), 67–68. https://doi.org/10.15406/hij.2023.07.00277
4. Kongor, J. E., Owusu, M., & Oduro-Yeboah, C. (2024). Cocoa production in the 2020s: challenges and solutions. CAB Agriculture and Bioscience. https://doi.org/10.1186/s43170-024-00310-6
5. Fabrice, Z. A., Fulbert, O. K., & Abdoulaye, T. (2023). Nutritive and Antioxidant Properties of Cocoa Placenta Obtained from Cocoa Varieties Grown in Lodjiboua (Côte d'Ivoire). Asian Journal of Advances in Agricultural Research, 22(1), 38–45. https://doi.org/10.9734/ajaar/2023/v22i1432
6. Ioannone, F., Di Mattia, C. D., De Gregorio, M., Sergi, M., Serafini, M., & Sacchetti, G. (2015). Flavanols, proanthocyanidins and antioxidant activity changes during cocoa (Theobroma cacao L.) roasting as affected by temperature and time of processing. Food Chemistry, 174, 256-262. https://doi.org/10.1016/j.foodchem.2014.11.019
7. Talbot, J. M. (2002). Tropical commodity chains, forward integration strategies and international inequality: coffee, cocoa and tea. Review of International Political Economy, 9(4), 701–734. https://doi.org/10.1080/0969229022000021862
8. Subroto, E., Djali, M., Indiarto, R., Lembong, E., & Baiti, N. (2023). Microbiological Activity Affects Post-Harvest Quality of Cocoa (Theobroma cacao L.) Beans. Horticulturae, 9(7), 805. https://doi.org/10.3390/horticulturae9070805
9. Ran, L.-X., Wei, X.-Y., Ren, E.-F., Qin, J.-F., Rasheed, U., & Chen, G.-L. (2025). Application of Microbial Fermentation in Caffeine Degradation and Flavor Modulation of Coffee Beans. Foods, 14(15), 2606. https://doi.org/10.3390/foods14152606
10. Quelal, O. M., Hurtado, D. P., Benavides, A. A., Alanes, P. V., & Alanes, N. V. (2023). Key Aromatic Volatile Compounds from Roasted Cocoa Beans, Cocoa Liquor, and Chocolate. Fermentation, 9(2), 166. https://doi.org/10.3390/fermentation9020166
11. Owusu, M., Petersen, M. A., & Heimdal, H. (2011). Relationship of sensory and instrumental aroma measurements of dark chocolate as influenced by fermentation method, roasting and conching conditions. Journal of Food Science and Technology, 50(5), 909–917. https://doi.org/10.1007/s13197-011-0420-2
12. da Silva Cota, A., de Freitas, R. S. G., Lefèvre, F., & Stedefeldt, E. (2023). Food handlers' lack of knowledge, and misunderstanding of safe food temperatures: An analysis using the theory of social representations. *Food Research International*, 174, 113486. https://doi.org/10.1016/j.foodres.2023.113486
13. Sentellas, S., & Saurina, J. (2023). Authentication of cocoa products based on profiling and fingerprinting approaches: Assessment of geographical, varietal, agricultural and processing features. *Foods*, 12(16), 3120. https://doi.org/10.3390/foods12163120
14. Hammerstone, J. F., Lazarus, S. A., Mitchell, A. E., Rucker, R., & Schmitz, H. H. (1999). Identification of Procyanidins in Cocoa (Theobroma cacao) and Chocolate Using High-Performance Liquid Chromatography/Mass Spectrometry. Journal of Agricultural and Food Chemistry, 47(2), 490–496. https://doi.org/10.1021/jf980760h
15. Toro-Uribe, S., Ibañez, E., Decker, E. A., Villamizar-Jaimes, A. R., & López-Giraldo, L. J. (2020). Food-Safe Process for High Recovery of Flavonoids from Cocoa Beans: Antioxidant and HPLC-DAD-ESI-MS/MS Analysis. Antioxidants, 9(5), 364. https://doi.org/10.3390/antiox9050364
16. Coulibaly, A., Dembele, A., Bohoussou, K., Toure, A., & Biego, G. (2014). Sampling of Cocoa Beans and Quantification of Ochratoxin A: Validation of the Methods. British Journal of Applied Science & Technology, 4(35), 4908–4917. https://doi.org/10.9734/bjast/2014/11562
17. Mishra, R. K., Catanante, G., Hayat, A., & Marty, J.-L. (2016). Evaluation of extraction methods for ochratoxin A detection in cocoa beans employing HPLC. Food Additives & Contaminants: Part A, 33(3), 500–508. https://doi.org/10.1080/19440049.2015.1133933
18. Bae, H., Jayaprakasha, G. K., Jifon, J., & Patil, B. S. (2012). Extraction efficiency and validation of an HPLC method for flavonoid analysis in peppers. Food Chemistry, 130(3), 751–758. https://doi.org/10.1016/j.foodchem.2011.07.041
19. Urbańska, B., Kowalska, J., & Miarka, D. (2018). Supply chain and traceability in the processing of cocoa beans. Zeszyty Problemowe Postepów Nauk Rolniczych, 594, 99-111. https://doi.org/10.22630/zppnr.2018.594.29
20. Bhatti, U. A., Tang, H., Wu, G., Marjan, S., & Hussain, A. (2023). Deep learning with graph convolutional networks: An overview and latest applications in computational intelligence. *International Journal of Intelligent Systems*, 2023(1), 8342104. https://doi.org/10.1155/2023/8342104
21. Eric, O., Gyening, R. M. O. M., Appiah, O., Takyi, K., & Appiahene, P. (2023). Cocoa beans classification using enhanced image feature extraction techniques and a regularized Artificial Neural Network model. *Engineering Applications of Artificial Intelligence*, 125, 106736. https://doi.org/10.1016/j.engappai.2023.106736
22. Pal, C., Das, S., Akuli, A., Adhikari, S. K., & Dey, A. (2024). Cocoa-Net: Performance Analysis on Classification of Cocoa Beans Using Structural Image Feature. Informatica, 48(12). https://doi.org/10.31449/inf.v48i12.5762
23. Kerkkamp, D., Bukhsh, Z., Zhang, Y., & Jansen, N. (2022). Grouping of Maintenance Actions with Deep Reinforcement Learning and Graph Convolutional Networks. Proceedings of the 14th International Conference on Agents and Artificial Intelligence, 574–585. https://doi.org/10.5220/0010907500003116
24. Usmani, I. A., Qadri, M. T., Zia, R., Alrayes, F. S., Saidani, O., & Dashtipour, K. (2023). Interactive effect of learning rate and batch size to implement transfer learning for brain tumor classification. *Electronics*, 12(4), 964. https://doi.org/10.3390/electronics12040964
25. Rajkumar, K., & Paramasivan, B. (2024). Energy Efficient Routing Mechanism Based on Similarity Guided Graph Neural Network and Decision Tree with Golden Eagle Optimization in VSN. Peer-to-Peer Networking and Applications, 17(5), 3408–3423. https://doi.org/10.1007/s12083-024-01747-2

26. Hussain, W., Mushtaq, M. F., Shahroz, M., Akram, U., Ghith, E. S., Tlija, M., & Ashraf, I. (2025). Ensemble genetic and CNN model-based image classification by enhancing hyperparameter tuning. *Scientific Reports*, 15(1), 1003. https://doi.org/10.1038/s41598-024-76178-3
27. Chen, Y. T., Chen, Y. L., Chen, Y. Y., Huang, Y. T., Wong, H. F., Yan, J. L., & Wang, J. J. (2022). Deep learning–based brain computed tomography image classification with hyperparameter optimization through transfer learning for stroke. *Diagnostics*, 12(4), 807. https://doi.org/10.3390/diagnostics12040807
28. Gao, J., Guo, J., Yuan, F., Yi, T., Zhang, F., Shi, Y., & Meng, Y. (2024). An exploration into the fault diagnosis of analog circuits using enhanced golden eagle optimized 1D-Convolutional neural network (CNN) with a time-frequency domain input and attention mechanism. *Sensors*, 24(2). https://doi.org/10.3390/s24020390
29. Anilkumar, P., Venugopal, P., Maddikunta, P. K. R., Gadekallu, T. R., Al-Rasheed, A., Abbas, M., & Soufiene, B. O. (2023). An adaptive DeepLabv3+ for semantic segmentation of aerial images using improved golden eagle optimization algorithm. *IEEE Access*, 11, 106688-106705. https://doi.org/10.1109/ACCESS.2023.3318867
30. Charlebois, S., Latif, N., Ilahi, I., Sarker, B., Music, J., & Vezeau, J. (2024). Digital traceability in agri-food supply chains: A comparative analysis of OECD member countries. *Foods*, 13(7), 1075. https://doi.org/10.3390/foods13071075
31. Muharromah, M. D., Kristiana, A. I., Slamin, Dafik, Agustin, I. H., & Baihaki, R. I. (2024). The analysis of the implementation of convolutional neural network architectures for coffee leaf disease image classification. In *AIP Conference Proceedings* (Vol. 3176, No. 1, p. 030035). AIP Publishing LLC. https://doi.org/10.1063/5.0225425
32. Harvyanti, A. F. M., Baihaki, R. I., Dafik, Ridlo, Z. R., & Agustin, I. H. (2023). Application of convolutional neural network for identifying cocoa leaf disease. In *Proceedings of the 1st International Conference on Neural Networks and Machine Learning 2022* (ICONNSMAL 2022) (Vol. 177, p. 283). Springer Nature.
33. Baihaki, R. I., Agustin, I. H., Ridlo, Z. R., & Kurniawati, E. Y. (2023). The comparison of convolutional neural networks architectures on classification potato leaf diseases. In *1st International Conference on Neural Networks and Machine Learning 2022* (ICONNSMAL 2022) (pp. 125-145). Atlantis Press.
34. Utami, W. W., Slamin, Dafik, Agustin, I. H., Maylisa, I. N., & Baihaki, R. I. (2024). Detecting railway sleeper damage using convolutional neural network equipped by Quadcopter drone. In *AIP Conference Proceedings* (Vol. 3176, No. 1, p. 030033). AIP Publishing LLC. https://doi.org/10.1063/5.0225338
35. Safdar, M. F., Nowak, R. M., & Pałka, P. (2022). A denoising and fourier transformation-based spectrograms in ecg classification using convolutional neural network. Sensors, 22(24), 9576. https://doi.org/10.3390/s22249576
36. Fang, Q., Li, Q., Song, Q., Montresor, S., Picart, P., & Xia, H. (2024). Convolutional and fourier neural networks for speckle denoising of wrapped phase in digital holographic interferometry. Optics Communications, 550, 129955. https://doi.org/10.1016/j.optcom.2023.129955
37. Hu, Z., Huang, J., Hu, D., & Wang, Z. (2022). A time-frequency image denoising method via neural networks for radar waveform recognition. IEEE Communications Letters, 27(1), 150-154. https://doi.org/10.1109/LCOMM.2022.3197979
38. Sedov, E. V., Freire, P. J., Seredin, V. V., Kolbasin, V. A., Kamalian-Kopae, M., Chekhovskoy, I. S., & Prilepsky, J. E. (2021). Neural networks for computing and denoising the continuous nonlinear Fourier spectrum in focusing nonlinear Schrödinger equation. Scientific Reports, 11(1), 22857. https://doi.org/10.1038/s41598-021-02252-9
39. Han, Y., & Hong, B. W. (2021). Deep learning based on Fourier Convolutional Neural Network incorporating Random Kernels. Electronics, 10(16), 2004. https://doi.org/10.3390/electronics10162004
40. Sedik, A., Marey, M., & Mostafa, H. (2023). WFT-Fati-Dec: enhanced fatigue detection AI system based on wavelet denoising and fourier transform. Applied Sciences, 13(5), 2785. https://doi.org/10.3390/app13052785
41. Hulliyah, K. (2023). Revolutionizing Digit Image Recognition: Pushing the Limits with Simple CNN and Challenging Image Augmentation Techniques on MNIST. Journal of Applied Data Sciences, 4(3), 119–129. https://doi.org/10.47738/jads.v4i3.104
42. Turkoglu, H., Arditi, D., & Polat, G. (2025). Golden eagle optimizer-based multi-objective optimization model for scheduling construction projects. Construction Management and Economics, 43(9), 704–722. https://doi.org/10.1080/01446193.2025.2502461
43. Shyla, S. I., Bell, T. B., & Sheela, C. J. J. (2023). Adaptive golden eagle optimization based multi-objective scientific workflow scheduling on multi-cloud environment. Multimedia Tools and Applications, 83(16), 47175–47198. https://doi.org/10.1007/s11042-023-17405-3
44. Al-Gburi, Z. D. S., & Kurnaz, S. (2022). Optical disk segmentation in human retina images with golden eagle optimizer. Optik, 271, 170103. https://doi.org/10.1016/j.ijleo.2022.170103
45. Wang, H., & Kim, D.-H. (2024). Graph Neural Network-Based Speech Emotion Recognition: A Fusion of Skip Graph Convolutional Networks and Graph Attention Networks. Electronics, 13(21), 4208. https://doi.org/10.3390/electronics13214208
46. Ding, Y., & Wang, X. (Cara). (2022). Multi-Dimensional Origin-Destination Freight Flow Prediction Via a Hybrid Multi-Graph Convolutional Neural Networks Based Model. SSRN Electronic Journal. https://doi.org/10.2139/ssrn.4211064
47. Pandey, G. K., & Srivastava, S. (2023). ResNet-18 comparative analysis of various activation functions for image classification. 2023 International Conference on Inventive Computation Technologies (ICICT), 595–601. https://doi.org/10.1109/icict57646.2023.10134464
48. Lopes, F., Agnelo, J., Teixeira, C. A., Laranjeiro, N., & Bernardino, J. (2020). Automating orthogonal defect classification using machine learning algorithms. Future Generation Computer Systems, 102, 932–947. https://doi.org/10.1016/j.future.2019.09.009
49. Chicco, D., & Jurman, G. (2020). The advantages of the Matthews correlation coefficient (MCC) over F1 score and accuracy in binary classification evaluation. BMC Genomics, 21(1). https://doi.org/10.1186/s12864-019-6413-7
50. Bowers, A. J., & Zhou, X. (2019). Receiver Operating Characteristic (ROC) Area Under the Curve (AUC): A Diagnostic Measure for Evaluating the Accuracy of Predictors of Education Outcomes. Journal of Education for Students Placed at Risk (JESPAR), 24(1), 20–46. https://doi.org/10.1080/10824669.2018.1523734
51. Maxwell, A. E., Warner, T. A., & Guillén, L. A. (2021). Accuracy Assessment in Convolutional Neural Network-Based Deep Learning Remote Sensing Studies—Part 1: Literature Review. Remote Sensing, 13(13), 2450. https://doi.org/10.3390/rs13132450
52. Poojary, R., & Pai, A. (2019). Comparative Study of Model Optimization Techniques in Fine-Tuned CNN Models. 2019 International Conference on Electrical and Computing Technologies and Applications (ICECTA), 1–4.

https://doi.org/10.1109/icecta48151.2019.8959681
53. Jiang, Z., Han, Z., Zhu, M., Wan, X., & Zhang, L. (2023). Effects of thermal processing on transformation of polyphenols and flavor quality. Current Opinion in Food Science, 51, 101014. https://doi.org/10.1016/j.cofs.2023.101014
54. Lin, Y. C., Choong, Y. M., & Chu, H. L. (2021). Effects of processing time and temperature on flavanol and procyanidin, proanthocyanidin and antioxidant activity of cocoa bean in Taiwan. Journal of Food and Nutrition Research, 9(1), 10-17. https://doi.org/10.12691/jfnr-9-1-2
55. Wong, K. Y., & Chung, F. (2019). Visualizing Time Series Data with Temporal Matching Based t-SNE. 2019 International Joint Conference on Neural Networks (IJCNN), 1–8. https://doi.org/10.1109/ijcnn.2019.8851847
56. Zeiler, M. D., Fergus, R. (2014). Visualizing and Understanding Convolutional Networks. Computer Vision – ECCV 2014, 818–833. https://doi.org/10.1007/978-3-319-10590-1_53
57. Kobak, D., & Berens, P. (2019). The art of using t-SNE for single-cell transcriptomics. Nature Communications, 10(1). https://doi.org/10.1038/s41467-019-13056-x
58. Wattenberg, M., Viégas, F., & Johnson, I. (2016). How to Use t-SNE Effectively. Distill, 1(10). https://doi.org/10.23915/distill.00002
59. Mirjalili, S., & Lewis, A. (2016). The Whale Optimization Algorithm. Advances in Engineering Software, 95, 51–67. https://doi.org/10.1016/j.advengsoft.2016.01.008
60. Zhang, L., Peng Lim, C., & Liu, C. (2023). Enhanced bare-bones particle swarm optimization based evolving deep neural networks. Expert Systems with Applications, 230, 120642. https://doi.org/10.1016/j.eswa.2023.120642
61. He, K., Zhang, X., Ren, S., & Sun, J. (2016). Deep Residual Learning for Image Recognition. 2016 IEEE Conference on Computer Vision and Pattern Recognition (CVPR), 770–778. https://doi.org/10.1109/cvpr.2016.90
62. Louis Uzoegwu Farah, C. (2023). Comparative Analysis for Predicting Cardiovascular Diseases Using Machine Learning and Deep Learning Approaches. International Journal of Science and Research (IJSR), 12(8), 945–964. https://doi.org/10.21275/sr23809044938
63. Mohammadi-Balani, A., Dehghan Nayeri, M., Azar, A., & Taghizadeh-Yazdi, M. (2021). Golden eagle optimizer: A nature-inspired metaheuristic algorithm. Computers & Industrial Engineering, 152, 107050. https://doi.org/10.1016/j.cie.2020.107050
64. Krämer, K., Müller, S., & Kosterhon, M. (2025). Deep Learning-Tuned Adaptive Inertia Weight in Particle Swarm Optimization for Medical Image Registration. Proceedings of the 20th International Joint Conference on Computer Vision, Imaging and Computer Graphics Theory and Applications, 307–318. https://doi.org/10.5220/0013122000003912
65. Kiranyaz, S., Ince, T., & Gabbouj, M. (2013). Particle Swarm Optimization. Multidimensional Particle Swarm Optimization for Machine Learning and Pattern Recognition, 45–82. https://doi.org/10.1007/978-3-642-37846-1_3
66. Leticio, G., Santos, M., Valem, L., Kawai, V., Breve, F., & Pedronette, D. (2025). Graph Convolutional Networks and Particle Competition and Cooperation for Semi-Supervised Learning. Proceedings of the 20th International Joint Conference on Computer Vision, Imaging and Computer Graphics Theory and Applications, 519–526. https://doi.org/10.5220/0013267000003912
67. Huang, Y., & Albert C. S., C. (2020). Semi-Supervised Multimodality Learning With Graph Convolutional Neural Networks For Disease Diagnosis. 2020 IEEE International Conference on Image Processing (ICIP), 2451–2455. https://doi.org/10.1109/icip40778.2020.9191172
68. Zhuang, C., & Ma, Q. (2018). Dual Graph Convolutional Networks for Graph-Based Semi-Supervised Classification. Proceedings of the 2018 World Wide Web Conference on World Wide Web - WWW '18, 499–508. https://doi.org/10.1145/3178876.3186116
69. Suzuki, T., Yasuda, Y., Nakamura, R., & Ohsaki, H. (2020). On Estimating Communication Delays using Graph Convolutional Networks with Semi-Supervised Learning. 2020 International Conference on Information Networking (ICOIN), 481–486. https://doi.org/10.1109/icoin48656.2020.9016603
70. Lang, Y., & Gao, Y. (2025). Dream Optimization Algorithm (DOA): A novel metaheuristic optimization algorithm inspired by human dreams and its applications to real-world engineering problems. Computer Methods in Applied Mechanics and Engineering, 436, 117718. https://doi.org/10.1016/j.cma.2024.117718
71. Zhang, Y., & Jin, Z. (2020). Group teaching optimization algorithm: A novel metaheuristic method for solving global optimization problems. Expert Systems with Applications, 148, 113246. https://doi.org/10.1016/j.eswa.2020.113246
72. Heidari, N., & Iosifidis, A. (2021). Progressive Graph Convolutional Networks for Semi-Supervised Node Classification. IEEE Access, 9, 81957–81968. https://doi.org/10.1109/access.2021.3085905
73. Mortazavi, A., Toğan, V., & Nuhoğlu, A. (2018). Interactive search algorithm: A new hybrid metaheuristic optimization algorithm. Engineering Applications of Artificial Intelligence, 71, 275–292. https://doi.org/10.1016/j.engappai.2018.03.003
74. Razi, N., Bagheri, R., & Pourabbas, H. (2024). Metaheuristic-Driven Optimization for Complex Multidimensional Decision-Making: Journal of Accounting, Business and Management (JABM), 31(1), 38. https://doi.org/10.31966/jabminternational.v31i1.1314
75. Parida, R. N. R., Singh, B. K., & Pradhan, C. (2025). A Hybrid Image Encryption Technique for Grayscale and Color Image Using Tinkerbell and Arnold Cat Map. SN Computer Science, 6(5). https://doi.org/10.1007/s42979-025-04059-1